PLCG1 is required for AML1-ETO leukemia stem cell self-renewal

Schnoeder, Tina M; Schwarzer, Adrian; Jayavelu, Ashok Kumar; Hsu, Chen-Jen; Kirkpatrick, Joanna; Döhner, Konstanze; Perner, Florian; Eifert, Theresa; Huber, Nicolas; Arreba-Tutusaus, Patricia; Dolnik, Anna; Assi, Salam A; Nafria, Monica; Jiang, Lu; Dai, Yu-Ting; Chen, Zhu; Chen, Sai-Juan; Kellaway, Sophie G; Ptasinska, Anetta; Ng, Elizabeth S

DOI:
10.1182/blood.2021012778

PLCG1 is required for AML1-ETO leukemia stem cell self-renewal

Short title: AML1-ETO LSC function depends on PLCG1

Tina M. Schnoeder[1], Adrian Schwarzer[2,3], Ashok Kumar Jayavelu[4], Chen-Jen Hsu[1], Joanna Kirkpatrick[5], Konstanze Döhner[6], Florian Perner[1,7], Theresa Eifert[1], Nicolas Huber[1], Patricia Arreba-Tutusaus[8], Anna Dolnik[9], Salam A. Assi[10], Monica Nafria[10], Lu Jiang[11], Yu-Ting Dai[11], Zhu Chen[11], Sai-Juan Chen[11], Sophie G. Kellaway[10], Anetta Ptasinska[10], Elizabeth S. Ng[12], Edouard G. Stanley[12,13], Andrew G. Elefanty[12], Marcus Buschbeck[14] , Holger Bierhoff [15], Steffen Brodt[16], Georg Matziolis[16], Klaus-Dieter Fischer[17], Andreas Hochhaus[18], Chun-Wei Chen[19], Olaf Heidenreich[20,21], Matthias Mann[4], Steven W. Lane[22], Lars Bullinger[9], Alessandro Ori[5], Björn von Eyss[5], Constanze Bonifer[10,23] and Florian H. Heidel[1,5,18,23,24]

1 Innere Medizin C, Hämatologie, Onkologie, Stammzelltransplantation und Palliativmedizin, Universitätsmedizin Greifswald, Greifswald 17475, Germany
2 Department of Hematology, Hemostaseology, Oncology and Stem Cell Transplantation, Hannover Medical School, Hannover 30625, Germany
3 Institute of Experimental Hematology, Hannover Medical School, Hannover 30625, Germany
4 Max-Planck-Institute of Biochemistry, Munich, Germany
5 Leibniz Institute on Aging, Fritz-Lipmann Institute (FLI), Jena 07745, Germany
6 Department of Internal Medicine III, University Hospital Ulm, Ulm 89070, Germany
7 Department of Pediatric Oncology, Dana Farber Cancer Institute, Harvard University, Boston, MA 02215, USA
8 Department of Oncology, Hematology, Immunology, and Rheumatology, University Hospital Tübingen, Tübingen 72076, Germany
9 Hematology, Oncology and Tumor Immunology, Charité University Medicine, Berlin 13353, Germany
10 Institute for Cancer and Genomic Sciences, University of Birmingham, Birmingham B152TT, UK
11 State Key Laboratory of Medical Genomics, Shanghai Institute of Hematology, National Research Center for Translational Medicine, Ruijin Hospital affiliated to Shanghai Jiao Tong University School of Medicine, 200025 Shanghai, China
12 Murdoch Children's Research Institute, The Royal Children's Hospital, Flemington Road, Parkville, Victoria 3052, Australia
13 Department of Paediatrics, Faculty of Medicine, Dentistry and Health Sciences, University of Melbourne Parkville, Victoria 3052, Australia
14 Josep Carreras Leukemia Research Institute, Badalona 08916, Spain
15 Institute of Biochemistry and Biophysics, Center for Molecular Biomedicine, Friedrich-Schiller University, Jena 07745, Germany
16 University Hospital Jena, Orthopaedic Department at Campus Eisenberg, Eisenberg 07607, Germany
17 Institute for Cell Biology and Biochemistry, Otto-von-Guericke University, Magdeburg 39120, Germany
18 Innere Medizin 2, Hämatologie und Onkologie, Universitätsklinikum Jena, Germany
19 Department of Systems Biology, Beckman Research Institute of City of Hope, Duarte, CA, USA
20 Northern Institute for Cancer Research, University of Newcastle, Newcastle upon Tyne NE2 4HH, UK
21 Princess Maxima Center for Pediatric Oncology, Utrecht 3584CS, the Netherlands
22 QIMR Berghofer Medical Research Institute, Brisbane, QLD 4006, Australia
23 Senior Author
24 Lead contact

Correspondence:
Florian H. Heidel
Universitätsmedizin Greifswald, Sauerbruchstraße, 17489 Greifswald, Germany
florian.heidel@uni-greifswald.de
(t) +49-3834-86-6698, (f) +49-3834-86-6713

Keywords: AML1-ETO, PLCG1, Leukemia Stem Cells

Scientific category: Myeloid Neoplasia

Text word count: 4141
Abstract word count: 124
Number of figures: 7
Number of references: 44

KEYPOINTS

- Using a multi-omics approach, we uncover deregulation of PLCG1-signaling by an intergenic regulatory element in AML1-ETO driven AML.
- The AML1-ETO specific functional dependency on PLCG1 is essential for LSC self-renewal and facilitates therapeutic targeting.

ABSTRACT

In an effort to identify novel drugs targeting fusion-oncogene induced acute myeloid leukemia (AML), we performed high-resolution proteomic analysis. In AML1-ETO (AE) driven AML we uncovered a de-regulation of phospholipase C (PLC) signaling. We identified PLCgamma 1 (PLCG1) as a specific target of the AE fusion protein which is induced after AE binding to intergenic regulatory DNA elements. Genetic inactivation of *PLCG1* in murine and human AML inhibited AML1-ETO dependent self-renewal programs, leukemic proliferation, and leukemia maintenance *in vivo*. In contrast, PLCG1 was dispensable for normal hematopoietic stem- and progenitor cell function. These findings are extended to and confirmed by pharmacologic perturbation of Ca++-signaling in AML1-ETO AML cells, indicating that the PLCG1 pathway poses an important therapeutic target for AML1-ETO positive leukemic stem cells.

INTRODUCTION

Chromosomal translocations found in acute myeloid leukemia (AML) can generate oncogenic fusions with aberrant epigenetic and transcriptional functions. However, direct therapeutic targeting of leukemia fusion proteins has not been accomplished so far. Although high remission rates can be induced in patients diagnosed with AML1-ETO (AE)/t(8;21)-positive AML, only 45-70% of patients achieve long-term disease-free survival [1]. In these patients, the disease maintaining clone is not eliminated by chemotherapy, an effect that has been attributed to a persistent leukemia stem cell (LSC) pool. In AML, these LSCs share immunophenotypic features with normal hematopoietic stem cells (HSCs), reside in the bone marrow (BM), and may give rise to relapse after discontinuation of chemotherapy. One functional characteristic of LSCs is unlimited self-renewal capacity and several genes and signaling pathways have been identified to maintain the balance between stem cell self-renewal and differentiation [2]. Therefore, targeting the oncogene induced self-renewal capacity of LSCs could eventually eliminate the malignant clone and prevent relapse. In this study we addressed this issue and present a strategy that identified a therapeutic target directly regulating the maintenance of AE-positive LSCs.

MATERIALS & METHODS

Cell Lines

Leukemia cell lines were purchased from DSMZ (Braunschweig, Germany). Kasumi-1_Cas9-EGFP and SKNO-1_Cas9-Blast are subclones of Kasumi-1 and SKNO-1, respectively, and are stably transduced with either lentiCas9-EGFP (Addgene #63592) or lentiCas9-Blast (Addgene #52962).

Primary Patient Samples

Primary AML patient samples and healthy donor controls were obtained after informed consent and according to the Helsinki declaration within the AML-trials of the German-Austrian AMLSG study group and from the Hematology Tumor Bank Jena and Magdeburg, approved by the respective local ethics committees (University Hospitals Jena, Ulm or Magdeburg).

Animal Studies

Mice were housed under pathogen-free conditions in the Animal Research Facility OvGU, Magdeburg and University Hospital Jena, Germany. All experiments were conducted after approval by the Landesverwaltungsamt Sachsen-Anhalt (42502-2-1279 UniMD) and Thüringen (02-030/2016). Conditional Plcg1 mice B6(Cg)-Plcg1tm1Flh/J (Plcγ1 flox/flox) were generated by us as published before [3]. Retroviral induction of leukemia was performed as published previously [4,5]. For *in vivo* drug treatment, Cyclosporin A was diluted in NaCl0.9% and administered by s.c. injections (30 mg/KG) once daily. NaCl0.9% was injected as diluent control.

Immunohistochemistry

Spleen, liver and lung were fixed and embedded according to standard protocols. Slides were automatically processed for H&E staining (Leica AutoStainer XL, Leica Biosystems, Wetzlar, Germany). Images were acquired at 10x magnification on an AxioImager A.2 (Carl Zeiss Microscopy, Jena, Germany) and processed using the ImageJ software (NIH, Bethesda, MD, USA). To analyze cell morphology, $1x10^5$ cells were centrifuged onto glass slides and stained with May-Grünwald/Giemsa staining as described before [6].

Flow Cytometry and Antibody Staining

Immunophenotyping of normal and leukemic cell compartments and of leukemic PB and BM was performed as described before [4,7]. Antibodies are provided in Supplemental Table 1. Flow cytometry was performed on a FACS CantoII cytometer (Becton Dickinson, Heidelberg, Germany). Cell cycle analysis with Ki67/Hoechst and intracellular flow cytometry in human AML cell lines were performed using the Fix & Perm Cell Permeabilization Kit (Life Technologies, Darmstadt, Germany).

Genetic Inactivation by RNAi and CRISPR/Cas9

Genetic inactivation by RNAi was performed as previously described [6] unless otherwise stated. For knockdown of AML1-ETO, the SEW vector system with EGFP was used (provided by M. Scherr, Hannover Medical School, Germany [8]). For CRISPR/Cas9 experiments, guide RNAs targeting *PLCG1*, *ETO* and *RPA3* were designed using the Broad GPP tool [9]. sgRNA sequences are provided in Supplemental Table 2. For cloning of sgRNA sequences, the improved-scaffold-pU6-sgRNA-EF1Alpha-PURO-T2A-RFP (ipUSEPR) vector system [10], with puromycin resistance and RFP selection marker was used. Genetic inactivation by CRISPR/Cas9 was performed as published before [11]. For knockout of *JUN*, *CREB1* and *FOS*, Kasumi-1 cells were transduced with the single-vector lentiviral GeCKO system [12] containing sgRNAs for the respective genes, or a non-targeting control (Genescript Biotech, Piscataway Township, NJ, USA). Apoptosis was measured by flow cytometry as indicated using Annexin V / SYTOX®Blue staining following the manufacturer`s instruction. Primary mouse BM cells (AE/K, MA9), primary human BM cells isolated from AML patients or healthy donors, or human cell lines were seeded in methylcellulose according to standard protocols and as published previously [6,13].

Quantitative Real-Time PCR

Q-PCR experiments were performed as previously published [7,11]. Analysis of PLCG1 mRNA expression was performed in AE-positive human embryonic stem (ES) cells, human ES cells expressing a doxycyclin (Dox)-inducible AE-fusion gene [14]. Three independent ES cell clones were stimulated with or without Dox (0-10 ng/ml) and total RNA was isolated. Primer sequences are listed in Supplemental Table 3.

Protein Extraction and Immunoblotting

Western Blotting was performed according to standard protocols as previously published [6,13]. Whole bone marrow cells of Plcg1+/+ and Plcg1-/- mice were lysed as described previously [6]. Antibodies are indicated in Supplemental Table 1.

Proteome and Transcriptome Analyses

Global proteome and transcriptome profiling were performed and analyzed as previously described [11] unless otherwise stated. Proteome data from murine leukemia cells were searched against a species specific (*Mus musculus* or *Homo sapiens*) Swissprot database. Relative quantification was performed in Spectronaut for each pairwise comparison using the replicate samples from each condition. Detailed information on gene- and protein-expresssion analyses is provided in the supplement.

Statistics and analysis of gene expression data

Kaplan-Meier curves were plotted using GraphPad Prism™ version 7.00 (GraphPad Software, SanDiego, CA) using the log-rank test (Mantel-Cox test). Statistical analyses were performed using Student *t* test (normal distribution) or Mann-Whitney U test. *p* less than 0.05 was considered statistically significant. Affymetrix .cel files and sample annotation from published AML gene expression datasets GSE13204 [15], GSE14468 [16] and the HOVON AML cohort E-MTAB-3444 were downloaded from Gene Expression Omnibus (GEO) or EBI ArrayExpress, respectively. mRNA expression of PLC family members in AML was downloaded from BloodSpot data base (http://servers.binf.ku.dk/bloodspot/).

Data availability

Raw data files for the RNA-sequencing analysis and the LncRNA Microarray data have been deposited in the NCBI Gene Expression Omnibus (GEO) under accession number GSE120828 (RNA-Seq) and GSE122062 (LncRNA Microarray). The mass spectrometry data have been deposited to the ProteomeXchange Consortium (http://proteomecentral.proteomexchange.org) via the PRIDE partner repository [17,18] with the dataset identifier PXD011251 (patient samples, mouse LSCs) and PXD026374 (SKNO-1; reviewer-account: **Username:** reviewer_pxd026374@ebi.ac.uk, **Password:** l5WVfdbR).

RESULTS

Phospholipase C signaling is enriched in AML1-ETO LSCs

To identify oncogenic cellular functions with relevance for LSC self-renewal, we performed global proteome profiling. AML was induced by retroviral expression of either AML1-ETO (AE) or MLL-AF9 (MA9) in murine HSPCs (Lineage-Sca1+Kit+, LSK) which were subsequently transplanted into irradiated syngeneic recipients. After onset of AML, LSC-enriched (GFP+Kit+) cells isolated from 4 different primary recipient hosts were analyzed by in-depth quantitative proteomic analysis using high-resolution mass spectrometry (MS) (Figure 1A; supplemental Figure 1A-C). More than 3,000 proteins were quantified (supplemental Figure 1A) with 868 proteins being differentially expressed between AE and MA9 LSC-enriched populations (supplemental Figure 1C). Gene set enrichment analyses (GSEA) revealed a significant enrichment of calcium-dependent cellular functions in AE-LSCs (Figure 1B) with phospholipase C (PLC)- and Calcium-signaling being among the most highly enriched pathways (Figure 1C). To validate a role for the PLC-Calcium-axis in primary patient samples, we performed MS-based proteomics on sorted CD34+ blasts from four AE-positive versus four AE-negative AML patients (Figure 1D-E; supplemental Figure 1D-F) and GSEA confirmed de-regulation of Calcium-dependent cellular functions in the AE-positive samples (Figure 1F). We next sought to analyze the expression of PLCs in published AML gene expression datasets [15,16,19]. Out of 13 PLC-family members, only *PLCG1* expression was highly increased in AE-AML in several independent datasets (Figure 1G; supplemental Figure 2A-D), suggesting a functional relevance for AE-driven AML. Likewise, PLCG1 protein expression was increased in human AE-positive cell lines Kasumi-1 (supplemental Figure 2E) and SKNO-1 (Figure 1H; supplemental Figure 2F) and primary AE-AML (Figure 1I and supplemental Figure 2G) when compared to non-AE controls. Of note, high PLCG1 expression correlated with inferior relapse-free survival (Figure 1J) and was significantly elevated in patients experiencing relapse (Figure 1K), which indicates its potential relevance for the persistent LSC population.

PLCG1 is a target of AML1-ETO

To clarify whether high expression of *PLCG1* in AE-AML could be induced by AML1-ETO, we analyzed AML1-Chromatin-Immunoprecipitation (ChIP-) sequencing data from AE-positive SKNO-1 cells, non-AE cell line (K562) and normal human CD34+ cells (https://genome.ucsc.edu). Here, binding of AML1 could exclusively be detected at the *PLCG1* promoter region in SKNO-1 cells (Figure 2A). To understand the mechanism of *PLCG1* induction, we analyzed DNaseI hypersensitive site (DHS) and promoter-Capture Hi-C (CHi-C) data generated in Kasumi-1 cells, a well characterized and widely used model system for t(8;21) AML [20-23], in the presence (siMM; CTRL) or absence (siAE; shAE) of AML1-ETO and compared them to data generated from patient cells [24] (Figure 2B). The CHi-C data identified large numbers of DHSs interacting with the *PLCG1* promoter forming an extensive regulatory domain extending far upstream into the neighboring locus and beyond. AE-knockdown led to a reduction of *PLCG1*

expression as measured by RNA-Seq (Figure 2B). Consistent with these findings, inactivation of AE by RNAi in SKNO-1 and Kasumi-1 cells resulted in significant decrease of PLCG1 expression (Figure 2C).

To examine the transcription factor complexes regulating *PLCG1* and its response to AE-knockdown, we integrated these data with published ChIP-sequencing data [22,24,25] (Figure 2B). For the detection of AE binding, antibodies against the translocation partner ETO of the AML1-ETO fusion protein which is usually not expressed in Kasumi-1 cells [25] were used. We also examined binding of the transcription factors LMO2 and LDB1 which form a complex with AE and which is required for leukemogenesis [26], together with AML1 (RUNX1), the AML1-dependent transcription factors PU.1, C/EBPα, as well as Polymerase (POL) II, and H3K27 acetylation (H3K27ac). We also measured the binding of AP-1 (JUN/FOS) as the binding of this factor is strictly dependent on the presence of AE [23,25]. By integrating ChIP-seq with DNaseI-seq and RNA-seq data before (siMM; CTRL) and after (siAE; shAE) AML1-ETO knockdown, we identified several AE binding-sites at the *PLCG1* promoter as well as upstream (Figure 2B). Depletion of AE by RNAi resulted in decreased binding of AP-1, LMO2, reduction of POL II and the H3K27 acetylation mark at the promoter and reduced expression of *PLCG1* as seen by RNA-seq. C/EBPα was not recruited to the *PLCG1* locus prior to knockdown but bound to an AML1-ETO, AML1, ETS and AP-1 bound upstream element at -128 kb after depletion of AE (marked by a blue box). A detailed inspection of the enhancer sequence confirmed the presence of binding motifs for the above listed factors together with several other motifs (supplemental Figure 3A-C). The response of AML1 binding to AML1-ETO knockdown was cis-element-specific: binding was reduced at the -128 kb DHS and at the promoter but was increased at a DHS upstream of the *CHD6* gene that was not part of the *PLCG1* regulatory unit (Figure 2B). Taken together, our analysis demonstrates that AML1-ETO cooperates with different transcription factors to sustain high level expression of *PLGC1* in leukemic cells. To gain further insight into the role of AML1-ETO and to test whether induction of AML1-ETO was sufficient to activate *PLCG1*, we used a human embryonic stem (ES) cell differentiation model harboring a doxycycline (Dox)-inducible AML1-ETO [14]. Intriguingly, induction of AE-expression in multipotent progenitors derived from three independent ES cell clones (Figure 2D, lower panel) following exposure to Dox resulted in synchronous and gene-dosage dependent expression of *PLCG1* (Figure 2D, upper panel). Induction was accompanied by the binding of AML1-ETO to several pre-existing nuclease accessible sites at the regulatory upstream element and the promoter (Figure 2E) as determined by ATAC-Seq. Prior to induction, these sites were also bound by AML1.

An intergenic AML1-ETO binding non-coding element is essential for *PLCG1* expression

Our data from CHi-C experiments (Figure 2B) derived from Kasumi-1 [23] and primary t(8;21) AML patient cells [24], identified several genomic regions contacting the *PLCG1* promotor. The majority of the contacting genomic regions within a 200kb-range overlapped between Kasumi-1 and t(8;21) patient cells and were therefore considered specific contacts and thus enhancer candidates. To test, the role of such elements in AML1-ETO driven gene regulation, we performed CRISPR/Cas9 genome editing to excise the AE-bound 500 bp intergenic element at –128 kb that also

bound p300 in Kasumi-1 and SKNO-1 cells (Figure 3A). Targeting of the defined 500 bp region using 5 different sgRNA pairs effectively reduced *PLCG1* mRNA expression as compared to the non-targeting control (Figure 3B) and resulted in reduced colony numbers (Figure 3C) and size (supplemental Figure 4A) in methylcellulose. BET inhibitors are known to disrupt bromodomain and extra-terminal motif (BET) proteins to acetylated histones as well as transcription factors [27] and thereby prevent recruitment of RNA polymerase II to enhancer regions [28]. Treatment of Kasumi-1 and SKNO-1 cells with the BET-inhibitor JQ1 (Figure 3D) or the selective, highly potent and cell permeable BET-degrader dBET6 (Figure 3E) resulted in significant reduction of *PLCG1* expression. Likewise, pharmacologic p300 inhibition using Lys-CoA [29] led to attenuation of *PLCG1* expression (Figure 3F). Finally, we aimed to investigate whether high-level *PLCG1* expression directly depends on specific transcription factors known to be required for the activation of cell cycle regulators such as JUN, FOS and CREB and which are also required for the leukemic activity of t(8;21) cells *in vivo* [24,25]. CRISPR/Cas9-mediated genetic inactivation of *JUN*, *FOS* and *CREB* resulted in significant reduction of PLCG1 mRNA (Figure 3G; supplemental Figure 4B) and protein expression (supplemental Figure 4C). Consistently, depletion of AML1-ETO resulted in reduced binding of JUN to the *PLCG1* promotor in ChIP-seq experiments (Figure 3H). These data identify an AE bound enhancer that is important for *PCLG1* expression and provide conclusive evidence that AML1-ETO together with the signaling responsive factors AP-1 and CREB is required for the up-regulation of this gene in AE-cells.

AML1-ETO induced cellular functions depend on PLCG1

To assess the functional importance of PLCG1, we aimed to genetically inactivate *PLCG1* in human AE-leukemia. CRISPR/Cas9-mediated deletion (SKNO-1, Figure 4A; supplemental Figure 5A) or RNAi-mediated knockdown (Kasumi-1, Figure 4B; supplemental Figure 5B) of *PLCG1* impaired their proliferative capacity. Of note, this effect could be attributed to impaired proliferation rather than induction of apoptosis (supplemental Figure 5C-D). Consistently, loss of PLCG1 reduced colony forming unit (CFU) capacity *in vitro* (Figure 4C-D) and PLCG1-deficient Kasumi-1 cells showed impaired leukemia development *in vivo* (Figure 4E). These results indicate a functional role of PLCG1 in the proliferative capacity of leukemic cells harboring the AE fusion. Moreover, genetic inactivation of PLCG1 resulted in increased expression of myeloid markers such as CD13 and CD14, suggesting induction of differentiation in both AE cell lines (Figure 4F-G). When examining the transcriptome of PLCG1-depleted Kasumi-1 cells, GSEA revealed a strong induction of gene sets related to myeloid differentiation consistent with the differentiation phenotype observed before. In contrast, we observed down-regulation of gene sets linked to proliferation, stemness and c-Myc targets (Figure 4H). Testing the *PCLG1*-knockdown signature against more than 10,000 gene sets from MSigDB [30] revealed a remodeling of tumor cell metabolism with down-regulation of gene sets involved in regulating the cell cycle, transcription and splicing (supplemental Figure 5E). To investigate whether PLCG1 depletion would affect direct target genes of the AML1-ETO fusion gene, we next focused on genes that were directly bound and repressed by AML1-ETO in Kasumi-1 cells [22]. Strikingly, these AML1-ETO

repressed genes were strongly up-regulated upon *PLCG1* knockdown (Figure 4I-J), indicating that PLCG1 loss reversed the gene expression signature imposed by the AML1-ETO fusion gene in human AML cells. Consistently, these findings could be recapitulated by CRISPR-mediated deletion of *PLCG1* in SKNO-1 cells (Figure 4K).

AML1-ETO transformed cells depend on PLCG1

To understand the role of PLCG1-signaling in AE-LSCs, we had previously generated a knockout mouse model [3] (Figure 5A; supplemental Figure 6A) that allows conditional deletion of *Plcg1*. We used an oncogenic combination of AML1-ETO9a (AE) and mutated RAS (KRASG12D; K) (thereafter AE/K) which is clinically relevant [1] and results in a more aggressive phenotype [31]. Genetic deletion of *Plcg1* AE/K-LSCs (GFP+ LSK) by retroviral Cre-expression (Figure 5B) resulted in reduced colony formation and abrogated the AE-induced unlimited re-plating capacity *in vitro* (Figure 5C). Consistently, genetic deletion of *Plcg1* in AE/K-LSCs impaired leukemia development in secondary recipient hosts (Figure 5D-E). In contrast, deletion of *Plcg1* in MLL-AF9 (MA9) transformed LSKs did not affect colony formation and re-plating capacity to a major extent (Figure 5F), indicating a specific requirement of Plcg1 in AE-transformed LSC. Genetic deletion of *Plcg1* resulted in loss of stemness-associated genes in AML LSCs (e.g. *HOXA* genes, *MECOM*) and induction of a differentiation-associated signature (Figure 5G). GSEA confirmed loss of AE target genes and PLCG1 target genes identified in this analysis were negatively enriched in the AE-knockdown signature of Kasumi-1 cells (Figure 5H). Consistently, inactivation of *Plcg1* by RNAi in primary AE-transformed murine progenitors resulted in decreased colony numbers, induction of differentiation and limited re-plating capacity in methylcellulose (supplemental Figure 6B-D).

PLCG1 is required for maintenance of AML1-ETO LSCs but dispensable for normal HSC function

To experimentally confirm our previous findings and to assess the requirement for PLCG1 in maintenance of AE-LSCs *in vivo*, we injected unexcised AE/K-transformed Plcg1F/F Mx-Cre+ and Plcg1+/+ Mx-Cre+ leukemic cells into sublethally irradiated recipient hosts and monitored GFP+ cells at serial time points after transplantation (Figure 5I). By day 14 (and prior to Cre-induction by pIpC injection), equal abundance of GFP+ cells indicated comparable homing and engraftment of leukemic cells (Figure 5J). Following pIpC injection, the total number of AE/K Plcg1+/+ cells in each recipient mouse had increased until overt and lethal leukemia developed. Conversely, *Plcg1* deletion resulted in loss of leukemia development in 50% of recipient hosts and leukemic cells decreased below 1% in the peripheral blood until day 110 (Figures 5K). Overall, deletion of *Plcg1* resulted in significant reduction of disease penetrance and LSC numbers (GFP+ LSK cells; Figure 5L). Isolated LSCs from these animals revealed induction of differentiation (Figure 5M), loss of cell cycle activity (Figure 5N) and failed to re-establish disease in secondary recipient hosts (Figure 5O). Likewise, primary human t(8;21) AML cells showed impaired colony forming capacity following *PLCG1* inactivation *in vitro* (Figure 5P; supplemental Figure 6E). In contrast, genetic deletion of *Plcg1* (Figure 6A) appeared to be dispensable for steady-state hematopoiesis regarding peripheral blood

counts (Figure 6B) and immunophenotypic abundance of BM compartments at week 20 (Figure 6C-D). Likewise, normal murine hematopoietic stem cell (HSC) function was not impaired during serial transplantation as indicated by peripheral blood chimerism of primary and secondary recipient hosts (Figures 6E-I) and the abundance of HSPCs as determined in the BM of primary recipient hosts (Figure 6G-H). Consistently colony forming capacity of human HSC-enriched CD34+ BM cells was preserved in 3/5 and partially reduced in 2/5 donors (Figure 6J).

The fact that LSC with higher cell cycle activity than normal HSCs were sensitive to Plcg1 inhibition raised the possibility that these cells might exhaust faster under stress conditions. To address this question without using the transplantation system, we evaluated hematopoietic recovery and survival after serial injections of 5-fluorouracil (FU). When 5-FU was injected every 7 days to achieve depletion of regenerating progenitor cells, both wildtype and Plcg1-deficient mice displayed similar survival rates, with the majority of deaths occurring in week 4-5 (Figure 6K). When 5-FU was injected every second month to allow complete recovery of hematopoiesis, Plcg1-deficient mice showed a trend towards lower restoration of myeloid cells (Figure 6L) and decreased long-term survival (Figure 6M) only when stress is applied over several month. Together, these functional experiments demonstrate that AE but neither MA9-driven LSCs nor normal (steady-state) HSCs depend on PLCG1 to maintain their self-renewal capacity.

Pharmacologic perturbation of Ca++-signaling inhibits AML1-ETO LSC function

To date, no specific inhibitors of PLCG1 are available. To assess for relevant cellular functions that depend on PLCG1 in AE transformed cells, we performed in-depth proteomic analysis. PLCG1 was genetically deleted in AE positive SKNO-1 cells and global proteome was assessed following puromycin selection. We quantified hundreds of significantly differentially expressed proteins depending on the presence or absence of PLCG1. In particular, loss of PLCG1 significantly downregulated 412 proteins (Figure 7A; supplemental Figure 7A). GSEA identified cell signaling and specifically Ca++-signaling as relevant downstream functions affected by PLCG1 loss (Figure 7B). Consistently, previous reports [32] had suggested a functional relevance of PLCG1 for modulation of intracellular Ca++-homeostasis in hematopoietic and leukemic cells. Therefore, we aimed to confirm the effects of Ca++-signaling perturbation on AE-leukemia. First, we tested the efficacy of cyclosporin A (CsA), a clinically approved calcineurin inhibitor that blocks intracellular Ca++ release and activation of Ca++-dependent transcription programs [33] on leukemic cell lines. Here, Kasumi-1 and SKNO-1 cells showed significantly reduced proliferation upon CsA-treatment compared to non-AE cell lines HL-60 and OCI-AML3 (Figure 7C). To assess for AE-LSC function *in vivo*, we treated primary leukemic mice with established AE/K- or MA9-driven leukemia with CsA for 3 weeks (Figure 7D). Mice with established AE-leukemia showed reduction in total leukemic burden (Figures 7E-F; supplemental Figure 7B) and LSC numbers (Figure 7G). This reduction resulted in delayed disease onset and increased survival of secondary recipients hosts (Figure 7H). Notably, these effects could not be observed in MA9-driven leukemia (Figures 7I-L; supplemental Figure 7C), indicating specificity of this dependency for the AE-

fusion. To determine the functional abundance of LSCs and the leukemia initiating potential, we performed limiting dilution assays by injecting immunocompromised recipient mice with limiting numbers ($1x10^5$, $1x10^4$, $1x10^3$) of drug/diluent exposed GFP+ leukemic bone marrow cells. CsA exposed cells showed profound reduction in LSC frequency compared to diluent treated controls (Figure 7M-N, supplemental Figure 7D). Likewise, CsA treated primary human AE-positive AML blasts showed strong reduction in colony formation in methylcellulose (Figure 7O-P; supplemental Figure 7E) an effect that could not be observed with normal HSPCs derived from healthy donors (Figure 7Q) or other AML subtypes (supplemental Figure 7F-G). Consistently, *in vivo* treatment of primary human AE-leukemic cells in humanized mouse models resulted in reduced engraftment potential (Figure 7R-S, supplemental Figure 7H). Thus, pharmacologic perturbation of Ca++-signaling by CsA targets the AE-LSC compartment that is critical for development and maintenance of AE-AML.

DISCUSSION

AML1-ETO transforms HSPCs in a cell-type specific manner by conferring aberrant self-renewal capacity [34,35] and established AE-AML cells show a deregulation of a number of signaling pathways involved in leukemic maintenance [24,36,37]. In our study we identified *PLCG1* as an essential factor required for AE-AML. We show that this gene directly responds to the expression of AML1-ETO and we identified an enhancer that is required for LSC-specific expression. The mechanism of activation closely resembles activation of cell cycle regulators such as *CCND2* transcription by AML1-ETO [25] which also depends on presence of AP-1 transcription factors. These findings suggest that also *PLCG1* expression is regulated in a direct and indirect manner through AML1-ETO. Of note, disruption of gene-regulatory networks by genetic inactivation of the oncogenic fusion resulted in gradual and time-dependent changes of gene expression and modulated chromatin landscape.

Importantly, we found that PLCG1 function is specifically required for AML1-ETO LSCs but not for normal HSC function and that Calcium signaling downstream of PLCG1 is an essential component for leukemia maintenance.

Recent reports have described activation of PLCG1 in bulk leukemia populations and cell lines of t(8;21) AML and have linked its expression with resistance to chemotherapy [8]. Primary resistance, however, is not the major clinical limitation, as most patients with t(8;21) AML respond positively to chemotherapy [38]. In contrast, more than 50% eventually relapse or present with minimal residual disease that stays stable over many years [39]. Here, we show that PLCG1 is required for self-renewal properties and maintenance of AE-LSC and its inactivation depletes AE-transformed LSCs *in vivo*. We therefore hypothesize that PLCG1 plays an important role in the maintenance of a clinically relevant LSC pool that is responsible for relapse and thus highlights the relevant target population [1]. Corruption of the cellular signaling network by *PLCG1* upregulation is a part of the AE-specific transcriptional network and emphasize the importance of studying the gene regulatory networks of specific types of AML in detail to be able to uncover new therapeutic approaches.

Recent reports have highlighted the importance of tightly controlled Ca++-homeostasis for HSC self-renewal [40,41]. Such a requirement for tightly controlled Ca++ homeostasis may change during malignant transformation, depending on the oncogenic background. BCR-ABL transformed CML cells show activation of Wnt/Ca++/NFAT-signaling and pharmacologic abrogation of Ca++-signaling facilitates leukemia cell elimination when combined with tyrosine kinase inhibitor therapy [42]. In contrast, disturbance of Ca++-homeostasis through deletion of *Prdm16* results in delayed disease development and improved survival of recipient mice in MA9-transformed leukemia [43]. The fact that Ca++-signaling is functionally relevant specifically in t(8;21) AML allowed to use this information of devise a potential drug-repurposing regime for the eradication of AE-LSCs. Treatment with CsA delayed disease onset in secondary transplants, indicating that the LSC population is highly sensitive to this treatment and may form part of a sequential approach designed to prevent relapse.

In summary, our findings identified a critical pathway for AE-leukemia maintenance and self-renewal. As PLCG1 is dispensable for maintenance of normal HSPCs, we anticipate that targeting PLCG1-signaling will predict therapeutic success in AML1-ETO AML.

Acknowledgements

We thank A. Fenske (Central Animal Facility, Otto-von-Guericke University Magdeburg) and M. v.d. Wall (Animal Facility University Hospital Jena) for their support with animal care, R. Hartig (Flow Facility, Otto-von-Guericke University Magdeburg), M. Locke and K. Schubert (Flow Facility, Fritz-Lipmann Institute, Jena) for their support with cell sorting, L. Rothenburger (SF Histology, Fritz-Lipmann Institute, Jena) for support with histopathology, M. Scherr (Hannover Medical School, Hannover) for providing constructs, Peter Cockerill (Institute of Cancer and Genomic Sciences, University of Birmingham) for his help with motif annotation, N. Rahnis and P. Riemenschneider (CF Proteomics, Fritz-Lipmann Institute, Jena) for support with sample preparation and S. Frey and K. Kathner-Schaffert for technical assistance. We also thank Th. Fischer (OvGU Magdeburg) for helpful discussions during the initial steps of this project.

Authors Contributions

Conceptualization: T.M.S., F.H.H; Methodology: T.M.S., K.D.F., F.H.H.; Formal Analysis: T.M.S., A.S., A.K.J., J.K., A.D., T.E., N.H., C.J.H., C.B., S.A.A., L.L., Y.T.D., S.G.K., A.P., H.B., A.H., O.H., C.W.C., L.B., A.O., B.vE., F.H.H; Investigation: T.M.S., M.N.F., P.A.T; Resources: K.D., Z.C., S.J.C., S.B., G.M., E.N., E.S., A.E, M.M.; Writing-Original Draft: T.M.S., A.S., C.B., F.H.H.; Writing-Review & Editing: T.M.S., A.S., F.P., A.H., M.B., S.W.L., C.B., F.H.H.; Supervision: F.H.H.

Funding

This work was supported by grants of the German Research Council (DFG), (HE6233/6-1 to F.H. Heidel and SCHN1556/1-1 to T.M. Schnoeder), by a travel grant of the Fritz Thyssen Stiftung (Az. 50.19.0.003MN to T.M. Schnoeder), by the DFG-Collaborative Research Center (CRC854/2) to F.H. Heidel (Project A20), by the German Jose Carreras Leukemia Foundation (DJCLS F 12/06 to F.H. Heidel), and by the Thuringian state program ProExzellenz (RegenerAging - FSU-I-03/14) of the Thuringian Ministry for Research (to F.H. Heidel and H. Bierhoff). Research in C. Bonifer's lab is supported by a program grant from Bloodwise (15001) and a studentship grant from Universitas 21 for M. Nafria.

Declaration of interests: The authors declare no competing interests.

References

1. Papaemmanuil E, Gerstung M, Bullinger L, et al. Genomic Classification and Prognosis in Acute Myeloid Leukemia. *N Engl J Med*. 2016;374(23):2209-2221.

2. Lane SW, Gilliland DG. Leukemia stem cells. *Semin Cancer Biol*. 2010;20(2):71-76.

3. Saliakoura M, Rossi Sebastiano M, Pozzato C, et al. PLCgamma1 suppression promotes the adaptation of KRAS-mutant lung adenocarcinomas to hypoxia. *Nat Cell Biol*. 2020;22(11):1382-1395.

4. Heidel FH, Bullinger L, Feng Z, et al. Genetic and pharmacologic inhibition of beta-catenin targets imatinib-resistant leukemia stem cells in CML. *Cell Stem Cell*. 2012;10(4):412-424.

5. Mohr J, Dash BP, Schnoeder TM, et al. The cell fate determinant Scribble is required for maintenance of hematopoietic stem cell function. *Leukemia*. 2018;32(5):1211-1221.

6. Schnoder TM, Arreba-Tutusaus P, Griehl I, et al. Epo-induced erythroid maturation is dependent on Plcgamma1 signaling. *Cell Death Differ*. 2015;22(6):974-985.

7. Heidel FH, Bullinger L, Arreba-Tutusaus P, et al. The cell fate determinant Llgl1 influences HSC fitness and prognosis in AML. *J Exp Med*. 2013;210(1):15-22.

8. Mahmud H, Scherpen FJG, de Boer TM, et al. Peptide microarray profiling identifies phospholipase C gamma 1 (PLC-gamma1) as a potential target for t(8;21) AML. *Oncotarget*. 2017;8(40):67344-67354.

9. Doench JG, Hartenian E, Graham DB, et al. Rational design of highly active sgRNAs for CRISPR-Cas9-mediated gene inactivation. *Nat Biotechnol*. 2014;32(12):1262-1267.

10. Uckelmann HJ, Kim SM, Wong EM, et al. Therapeutic targeting of preleukemia cells in a mouse model of NPM1 mutant acute myeloid leukemia. *Science*. 2020;367(6477):586-590.

11. Jayavelu AK, Schnoder TM, Perner F, et al. Splicing factor YBX1 mediates persistence of JAK2-mutated neoplasms. *Nature*. 2020;588(7836):157-163.

12. Sanjana NE, Shalem O, Zhang F. Improved vectors and genome-wide libraries for CRISPR screening. *Nat Methods*. 2014;11(8):783-784.

13. Heidel F, Solem FK, Breitenbuecher F, et al. Clinical resistance to the kinase inhibitor PKC412 in acute myeloid leukemia by mutation of Asn-676 in the FLT3 tyrosine kinase domain. *Blood*. 2006;107(1):293-300.

14. Nafria M, Keane P, Ng ES, Stanley EG, Elefanty AG, Bonifer C. Expression of RUNX1-ETO Rapidly Alters the Chromatin Landscape and Growth of Early Human Myeloid Precursor Cells. *Cell Rep*. 2020;31(8):107691.

15. Haferlach T, Kohlmann A, Wieczorek L, et al. Clinical utility of microarray-based gene expression profiling in the diagnosis and subclassification of leukemia: report from the International Microarray Innovations in Leukemia Study Group. *J Clin Oncol*. 2010;28(15):2529-2537.

16. Wouters BJ, Lowenberg B, Erpelinck-Verschueren CA, van Putten WL, Valk PJ, Delwel R. Double CEBPA mutations, but not single CEBPA mutations, define a subgroup of acute myeloid leukemia with a distinctive gene expression profile that is uniquely associated with a favorable outcome. *Blood*. 2009;113(13):3088-3091.

17. Deutsch EW, Csordas A, Sun Z, et al. The ProteomeXchange consortium in 2017: supporting the cultural change in proteomics public data deposition. *Nucleic Acids Res*. 2017;45(D1):D1100-D1106.

18. Perez-Riverol Y, Csordas A, Bai J, et al. The PRIDE database and related tools and resources in 2019: improving support for quantification data. *Nucleic Acids Res*. 2019;47(D1):D442-D450.

19. Stavropoulou V, Kaspar S, Brault L, et al. MLL-AF9 Expression in Hematopoietic Stem Cells Drives a Highly Invasive AML Expressing EMT-Related Genes Linked to Poor Outcome. *Cancer Cell*. 2016;30(1):43-58.

20. Ben-Ami O, Friedman D, Leshkowitz D, et al. Addiction of t(8;21) and inv(16) acute myeloid leukemia to native RUNX1. *Cell Rep*. 2013;4(6):1131-1143.

21. Ptasinska A, Assi SA, Mannari D, et al. Depletion of RUNX1/ETO in t(8;21) AML cells leads to genome-wide changes in chromatin structure and transcription factor binding. *Leukemia*. 2012;26(8):1829-1841.

22. Ptasinska A, Assi SA, Martinez-Soria N, et al. Identification of a dynamic core transcriptional network in t(8;21) AML that regulates differentiation block and self-renewal. *Cell Rep*. 2014;8(6):1974-1988.

23. Ptasinska A, Pickin A, Assi SA, et al. RUNX1-ETO Depletion in t(8;21) AML Leads to C/EBPalpha- and AP-1-Mediated Alterations in Enhancer-Promoter Interaction. *Cell Rep*. 2019;28(12):3022-3031 e3027.

24. Assi SA, Imperato MR, Coleman DJL, et al. Subtype-specific regulatory network rewiring in acute myeloid leukemia. *Nat Genet*. 2019;51(1):151-162.

25. Martinez-Soria N, McKenzie L, Draper J, et al. The Oncogenic Transcription Factor RUNX1/ETO Corrupts Cell Cycle Regulation to Drive Leukemic Transformation. *Cancer Cell*. 2018;34(4):626-642 e628.

26. Sun XJ, Wang Z, Wang L, et al. A stable transcription factor complex nucleated by oligomeric AML1-ETO controls leukaemogenesis. *Nature*. 2013;500(7460):93-97.

27. Roe JS, Mercan F, Rivera K, Pappin DJ, Vakoc CR. BET Bromodomain Inhibition Suppresses the Function of Hematopoietic Transcription Factors in Acute Myeloid Leukemia. *Mol Cell*. 2015;58(6):1028-1039.

28. Gibbons HR, Mi DJ, Farley VM, Esmond T, Kaood MB, Aune TM. Bromodomain inhibitor JQ1 reversibly blocks IFN-gamma production. *Sci Rep*. 2019;9(1):10280.

29. Wang L, Gural A, Sun XJ, et al. The leukemogenicity of AML1-ETO is dependent on site-specific lysine acetylation. *Science*. 2011;333(6043):765-769.

30. Subramanian A, Tamayo P, Mootha VK, et al. Gene set enrichment analysis: a knowledge-based approach for interpreting genome-wide expression profiles. *Proc Natl Acad Sci U S A*. 2005;102(43):15545-15550.

31. Zuber J, Radtke I, Pardee TS, et al. Mouse models of human AML accurately predict chemotherapy response. *Genes Dev*. 2009;23(7):877-889.

32. Fu G, Chen Y, Yu M, et al. Phospholipase C{gamma}1 is essential for T cell development, activation, and tolerance. *J Exp Med*. 2010;207(2):309-318.

33. Clipstone NA, Crabtree GR. Identification of calcineurin as a key signalling enzyme in T-lymphocyte activation. *Nature*. 1992;357(6380):695-697.

34. Licht JD. AML1 and the AML1-ETO fusion protein in the pathogenesis of t(8;21) AML. *Oncogene*. 2001;20(40):5660-5679.

35. Mulloy JC, Cammenga J, MacKenzie KL, Berguido FJ, Moore MA, Nimer SD. The AML1-ETO fusion protein promotes the expansion of human hematopoietic stem cells. *Blood*. 2002;99(1):15-23.

36. Goyama S, Schibler J, Gasilina A, et al. UBASH3B/Sts-1-CBL axis regulates myeloid proliferation in human preleukemia induced by AML1-ETO. *Leukemia*. 2016;30(3):728-739.

37. Vegi NM, Klappacher J, Oswald F, et al. MEIS2 Is an Oncogenic Partner in AML1-ETO-Positive AML. *Cell Rep*. 2016;16(2):498-507.

38. Paschka P, Schlenk RF, Weber D, et al. Adding dasatinib to intensive treatment in core-binding factor acute myeloid leukemia-results of the AMLSG 11-08 trial. *Leukemia*. 2018.

39. Miyamoto T, Weissman IL, Akashi K. AML1/ETO-expressing nonleukemic stem cells in acute myelogenous leukemia with 8;21 chromosomal translocation. *Proc Natl Acad Sci U S A*. 2000;97(13):7521-7526.

40. Luchsinger LL, de Almeida MJ, Corrigan DJ, Mumau M, Snoeck HW. Mitofusin 2 maintains haematopoietic stem cells with extensive lymphoid potential. *Nature*. 2016;529(7587):528-531.

41. Umemoto T, Hashimoto M, Matsumura T, Nakamura-Ishizu A, Suda T. Ca(2+)-mitochondria axis drives cell division in hematopoietic stem cells. *J Exp Med*. 2018;215(8):2097-2113.

42. Gregory MA, Phang TL, Neviani P, et al. Wnt/Ca2+/NFAT signaling maintains survival of Ph+ leukemia cells upon inhibition of Bcr-Abl. *Cancer Cell*. 2010;18(1):74-87.

43. Corrigan DJ, Luchsinger LL, Justino de Almeida M, Williams LJ, Strikoudis A, Snoeck HW. PRDM16 isoforms differentially regulate normal and leukemic hematopoiesis and inflammatory gene signature. *J Clin Invest*. 2018.

44. Hu Y, Smyth GK. ELDA: extreme limiting dilution analysis for comparing depleted and enriched populations in stem cell and other assays. *J Immunol Methods*. 2009;347(1-2):70-78.

Figure Legends

Figure 1. Phospholipase C and Ca++ signaling is enriched in AML1-ETO transformed LSCs. (A) Outline of the proteomic workflow. (B) Gene set enrichment analysis (GSEA) on murine MLL-AF9 (MLL9) and AML1-ETO (AE) LSCs (*n*=4 per genotype). (C) Ingenuity pathway analysis (IPA) on murine AML1-ETO transformed LSC compared to MLL-AF9 positive controls. (D) Schematic of proteome analysis of primary human AML1-ETO/t(8;21) AML (*n*=4 per genotype). (E) Molecular analysis of AML patient samples applied for proteomic analysis. (F) GSEA on human t(8;21) AML compared to non-t(8;21) controls. (G) t-SNE plot displaying the gene expression landscape of 641 AML patients of the HOVON cohort [19] with an overlay of different AML subtypes (left) with absolute PLCG1 expression values (right). (H) PLCG1 protein expression in AML1-ETO positive (Kasumi-1, SKNO-1) versus AML1-ETO negative human AML cell lines analyzed by intracellular flow cytometry (*n*=5 per cell line; one-way ANOVA). **(I)** Protein expression of AML patients harboring different mutations analyzed by super SILAC analysis. (J) Relapse-free survival (RFS, B) in patients with t(8;21) AML according to the expression level of *PLCG1*. Survival curves were estimated with the Kaplan-Meyer method and compared using a log-rank test. (K) Scatterplot depicting *PLCG1* expression levels in t(8;21) patients according to their relapse status (no relapse, n=33; relapse, n=27; unknown, n=2).

Figure 2. PLCG1 is a target of AML1-ETO. (A) AML1 ChIP-sequencing analysis on normal CD34+ cells, (BCR-ABL+) K562 and (AML1-ETO+) SKNO-1 cells (https://genome.ucsc.edu). (B) Screenshot displaying changes in PLCG1 transcript levels based on RNA-sequencing (RNA-Seq, blue). Binding patterns of AML1-ETO (AE), RUNX1, JunD, C/EBPa, LDB1, LMO2, PU.1, RNA-Polymerase II (POLII), H3K27ac and DHS at the *PLCG1* locus in Kasumi-1 or patient-derived cells based on ChIP-sequencing and DNaseI-sequencing as well as conservation at the *PLCG1* locus as aligned reads. Upper lines show promoter-Capture Hi-C (CHi-C) data generated in Kasumi-1 or patient-derived cells identifying DHSs interacting with the *PLCG1* promoter. All data following inactivation of AML1-ETO (siAE; shAE) compared to non-targeting control (siMM; CTRL) [22-25]. (C) Western blot analysis (left panel) and mRNA expression (right panel) in SKNO-1_Cas9-Blast cells (upper panel) following

CRISPR/Cas9 knockout using ETO-specific gRNA or a non-targeting control (gLuc) and in Kasumi-1 cells (lower panel) transduced with shRNA targeting AML1-ETO (AE) or empty vector control (shEV). *n*=3 independent experiments; representative blot images are shown. (D) mRNA expression of PLCG1 (upper panel) and AML1-ETO (lower panel) in human embryonic stem (ES) cell-derived definitive hematopoietic progenitors expressing a Dox-inducible AML1-ETO fusion (data from 3 independent ES cell clones are shown). (E) Human ES-cell derived definitive hematopoietic progenitors expressing a Dox-inducible AML1-ETO fusion. ChIP-seq analysis displaying AML1-ETO binding at the *PLCG1* locus (blue) without Dox (0 Dox) and after Dox treatment (5 ng/mL; 5 Dox) for 24 hours. Chromatin accessibility at the *PLCG1* locus (green) after Dox treatment as indicated by ATAC-seq.

Figure 3. An intergenic AML1-ETO binding non-coding element is essential for *PLCG1* expression. (A) Schematic model of the 500 bp intergenic element characterized by p300 and AML1-ETO binding sites (green) in Kasumi-1 cells. sgRNAs targeting this region are shown with arrows. (B) PLCG1 mRNA expression in Kasumi_Cas9-EGFP cells (left panel) and SKNO-1_Cas9-Blast cells (right panel) following CRISPR/Cas9-induced knockout of the 500 bp intergenic region using specific gRNAs or a non-targeting control (NT). *n*=3 independent experiments, in duplicate; paired *t*-test. (C) Colony forming assay of Kasumi-1_Cas9_EGFP cells (left panel) and SKNO-1_Cas9-Blast cells (right panel) (day 14) following genetic inactivation of the 500 bp enhancer region using specific sgRNAs compared to non-targeting control (NT). *n*=2 independent experiments. (D-F) mRNA expression of PLCG1 (normalized to Beta2-microglobulin) in Kasumi-1 and SKNO-1 cells after treatment with (D) JQ1 (1µM, 24h), (E) dBET6 (1µM, 24h) and (F) Lys-CoA (1µM, 24h) compared to diluent control (DMSO). *n*=4 independent experiments, in duplicate; paired *t*-test. (G) mRNA expression of PLCG1 in Kasumi-1 cells after knockout of *JUN* using CRISPR/Cas9 (gJUN #1 and #2) or a non-targeting control (NT). *n*=3 independent experiments, in triplicate; paired *t*-test. (H) Screenshot displaying binding patterns of AML1-ETO, JUN and CEBPa at the *PLCG1* locus in Kasumi-1 cells based on ChIP-seq. All data following inactivation of AML1-ETO (siAE) compared to non-targeting control (siMM). Relevant peaks are highlighted with boxes.

Figure 4. AML1-ETO induced cellular functions depend on PLCG1. (A-B) Proliferation assayed by cell counting after trypan blue exclusion for (A) SKNO-1_Cas9-Blast cells transduced with gRNAs targeting PLCG1, RPA3 or a non-targeting control (gLuc) and (B) Kasumi-1 cells transduced with shRNAs targeting PLCG1or a non-targeting control (shSCR). *n*=4-5 independent experiments, one-way ANOVA. Representative western blot images confirming PLCG1 depletion are shown (day 5 or day 7 post-infection). (C-D) CFU analysis in (C) SKNO-1_Cas9-Blast and (D) Kasumi-1 cells on day 14. *n*=4-6 independent experiments; paired *t-test*. (E) Kaplan-Meier survival curves of humanized NSGS recipient mice, *n*=14 mice for shPLCG1-1 or shPLCG1-2 versus *n*=10 mice for non-targeting control (shSCR); shown are three independent cohorts, Mantel-Cox test. (F-G) Quantitative analysis (left panel) and representative histograms (right panel) after flow-cytometric evaluation of CD14 and CD13 expression on (F) SKNO-1_Cas9-Blast cells transduced with gRNAs targeting PLCG1 or a non-targeting control (gLuc) and (G) Kasumi-1 cells transduced with shRNAs targeting PLCG1or a non-targeting control (shSCR). *n*=4 independent experiments; paired *t-test*. (H) GSEA of expression changes in 160 hematopoiesis and leukemia-associated gene sets in Kasumi-1 cells transduced with a PLCG1 shRNA (sh1-1) against a non-targeting control (*n*=4 for each group). Plotted are normalized enrichment scores (NES) against the log10 false discovery rate (*FDR*). *FDR* <0.1 is indicated by the vertical line. (I-J) GSEA showing up-regulation of genes bound and repressed by the AML1-ETO fusion protein in Kasumi-1 cells transduced with a PLCG1 shRNA against a non-targeting control. (K) GSEA of expression changes in 160 hematopoiesis and leukemia-associated gene sets in SKNO-1 cells transduced with a PLCG1 sgRNA against a non-targeting control (*n*=4 for each group). Plotted are normalized enrichment scores (NES) against the log10 false discovery rate (*FDR*). *FDR* <0.1 is indicated by the vertical line.

Figure 5. AML1-ETO transformed hematopoietic stem cells depend on PLCG1. (A) Targeting strategy for the conditional *Plcg1* knockout mouse model. Exons 3 to 5 are flanked with LoxP-sites (red triangles) to facilitate tissue-specific deletion. FRT-sites, green triangles. (B-F) GFP+Kit+ BM cells of Plcg1+/+ and Plcg1F/F AML1-ETO/KRAS (AE/K) or MLL-AF9 (MA9) primary recipients were sorted and retrovirally infected with a Cre-recombinase (MSCV-Cre-puro), followed by 24h of puromycin selection. (C) Serial re-plating in methylcellulose. Colony counts per plating over 6 weeks are depicted for AML1-ETO/KRAS. Representative pictures of colonies

(second plating). *n*=3 independent experiments, in duplicate; paired *t-test*. (D) Kaplan-Meier survival curves of recipient animals of AE/K transformed Plcg1+/+ (*n*=16 mice) versus Plcg1-/- (*n*=7 mice) LSCs, Mantel-Cox test. (E) Histologic analysis of liver, lung and spleen morphology in Plcg1+/+ or Plcg1-/- AML1-ETO9a/KRAS (AE/K) transformed secondary recipients. Representative images are shown. Scale bars, 100 µm. (F) Serial re-plating in methylcellulose. Colony counts per plating over 6 weeks are depicted for MLL-AF9. Representative pictures of colonies (second plating). *n*=3 independent experiments, in duplicate; paired *t-test*. (G) Heatmap of differentially expressed genes in AE/KRAS transformed Plcg1+/+ (*n*=2) versus Plcg1-/- (*n*=3) LSCs 48 hours after genetic deletion of *Plcg1*. Red zones represent higher gene expression (upregulation), and blue zones represent lower gene expression (downregulation). (H) GSEA indicating loss of AML1-ETO (RUNX1-RUNX1T1) target genes (upper panel) and negative enrichment of PLCG1 target genes (lower panel) in the AML1-ETO knockdown signature of Kasumi-1 cells. NES, normalized enrichment score; AE, AML1-ETO; MM, Mismatch control; NT, non-targeting control; k/d, knockdown. (I) Schematic representation of the experimental set-up to study the effects of *Plcg1* inactivation on AML1-ETO/KRAS (AE/K)- transformed LSCs *in vivo*. (J) Analysis of sublethally (7 Gy) irradiated 6-8-week old primary recipients of AE/K-transformed Plcg1+/+ and Plcg1F/F LSK cells. pIpC injections were administered i.p. as indicated by arrows. Immunophenotyping of (GFP+) leukemia cells in peripheral blood of primary recipient mice. Plcg1+/+ (*n*=9 mice) versus Plcg1-/- (*n*=9 mice). (K) Survival of primary recipient mice. Plcg1+/+ (*n*=12 mice) versus Plcg1-/- (*n*=12 mice). Mantel-Cox test. (L) Immunophenotyping of GFP+ bone marrow (BM) LSKs (Plcg1+/+ *n*=8 mice, Plcg1-/- *n*=9 mice; Mann-Whitney *U* test. (M) Cytospins (May-Grünwald/Giemsa staining) of GFP+ LSK cells following short-term (24h) culture *ex vivo*. (N) Cell cycle analysis (Ki67/Hoechst staining) of GFP+ LSK cells from primary recipient mice following genetic inactivation of *Plcg1 in vivo* (Plcg1+/+, *n*=6 mice versus Plcg1-/-, *n*=6 mice; Mann-Whitney *U* test. (O) Kaplan-Meier survival curves of secondary recipients of $2x10^6$ BM cells from primary Plcg1+/+ (*n*=11) and Plcg1-/- (*n*=10) recipient mice, Mantel-Cox test. (P) Colony formation of leukemic bone marrow cells derived from patients at primary diagnosis of t(8;21) positive AML (n=6 individual patients). Colony number following *PLCG1* depletion by RNAi (shPLCG1-1 and 1-2) compared to non-targeting control (shSCR).

Figure 6. PLCG1 is dispensable for normal HSC function. (A) Experimental protocol for investigation of steady-state hematopoiesis. (B) White blood count (WBC), hemoglobin (HGB), and platelets (PLT) following genetic inactivation of *Plcg1* (Plcg1-/-, *n*=6) for 16 weeks of steady-state hematopoiesis, compared to Plcg1+/+ controls (*n*=14). (C) Immunophenotypic quantification of mature myeloid (Gr-1 Mac-1; F4/80), B-lymphoid (B220; CD19) and T-lymphoid (CD3) bone marrow cells (Plcg1+/+, *n*=10; Plcg1-/-, *n*=6). (D) Immunophenotypic quantification of stem- and progenitor cell abundance, specifically of hematopoietic stem cells (HSC: CD150+ CD48- L-S+K+) and multipotent progenitors (MPP: CD150 low, CD48+ L-S+K+) (Plcg1+/+, *n*=10; Plcg1-/-, *n*=6). (E) Protocol for assessing impact of Plcg1 loss on LT-HSC function by serial transplantation. (F) Peripheral blood chimerism of primary recipient mice (Plcg1+/+, *n*=6; Plcg1-/-, *n*=11); shown are two independent cohorts. (G) Immunophenotypic quantification of mature myeloid (Gr-1), B-lymphoid (B220; CD19) and T-lymphoid (CD3) bone marrow cells (Plcg1+/+, *n*=6; Plcg1-/-, *n*=6) from primary recipients. (H) Immunophenotypic quantification of stem- and progenitor cell abundance, specifically of hematopoietic stem cells (HSC: CD150+ CD48- L-S+K+) and multipotent progenitors (MPP: CD150 low, CD48+ L-S+K+) (Plcg1+/+, *n*=6; Plcg1-/-, *n*=6). (I) Peripheral blood chimerism of secondary recipient mice (Plcg1+/+, *n*=10; Plcg1-/-, *n*=11); shown are two independent cohorts. (J) Colony count of BM cells derived from healthy donors. Genetic inactivation of *PLCG1* by shRNA compared to non-targeting control (shSCR). *n*=5, in duplicate. (K) Short-term stress analysis after serial 5-fluorouracil (5-FU) injections; Kaplan-Meier survival curve of Plcg1+/+ (*n*=9) and Plcg1-/- (*n*=7) mice injected intravenously (i.v.) with 150 mg/kG 5-FU (arrows) every 7 days. (L) Long-term stress analysis by serial 5-FU injections (2-monthly injections i.v.). Kinetics of hematopoietic recovery as measured by peripheral white blood count of Plcg1-/- (*n*=8) and Plcg1+/+ (*n*=5) mice during the 2-monthly 5-FU injection schedule. (M) Survival rates of Plcg1-/- (*n*=8) and Plcg1+/+ (*n*=5) mice during long-term 5-FU treatment.

Figure 7. Pharmacologic suppression of Ca++-signaling inhibits AML1-ETO LSC function *in vitro* and *in vivo.* (A) Unsupervised hierarchical clustering of significantly downregulated proteins following genetic inactivation of *PLCG1* by a specific gRNA in SKNO-1_Cas9-Blast cells. (B) Network map displaying the significantly enriched signaling pathways upon genetic inactivation of *PLCG1,* annotation from Reactome. The

node size and color represent number of proteins participating in each node. (C) Proliferation assayed by cell counting after trypan blue exclusion for Kasumi-1, SKNO-1, HL-60 and OCI-AML3 cells following treatment with the calcineurin inhibitor cyclosporin A (CsA, 5 µM) or diluent control (NaCl 0.9%). *n*=4 independent experiments, one-way ANOVA. (D) Analysis scheme of primary recipient mice following ciclosporin A (CsA) treatment vs. diluent control (NaCl 0.9%). (E) Spleen weight of AE/K primary recipient mice; Mann-Whitney *U* test. (F) Histologic analysis of liver, lung and spleen morphology after onset of AML in AE/K primary recipient mice treated with CsA or diluent control (NaCl 0.9%). Scale bars, 100 µm. (G) Immunophenotypic analysis of AE/K GFP+ BM LSK cells; Mann-Whitney U test. (H) Kaplan-Meier survival curves of AE/K secondary recipient mice. Irradiated (13 Gy, single dose) 6-8 week-old recipients of $2x10^6$ bone marrow cells from AE/K CsA (*n*=7) or NaCl 0.9% (*n*=8) treated primary recipients; Mantel-Cox test. (I) Spleen weight of MA9 primary recipient mice treated with CsA or diluent control (NaCl 0.9%), n.s.=not significant. (J) Histologic analysis of liver, lung and spleen morphology after onset of AML in MA9 primary recipient mice after treatment with CsA or diluent control. Scale bars, 100 µm. (K) Immunophenotypic analysis of GFP+LSK cells in the bone marrow of MA9 primary recipient mice, n.s.=not significant. (L) Survival of MA9-transformed secondary recipient mice. Irradiated (13 Gy, single dose) 6-8-week old recipients of $2x10^6$ bone marrow cells from MA9 CsA or NaCl 0.9% treated primary recipient mice (*n*=8 CsA; *n*=8 NaCl 0.9%), Mantel-Cox test. (M-N) Table (M) and graph (N) depicting the number of engrafted mice per dilution in the NaCl- vs. CsA-treated cohort. LSC frequency was 1/5801 for NaCl-treated recipients (95% confidence interval (CI), 1/2182-15427) and 1/121901 for CsA-treated recipients (95% confidence interval, 1/39911-372329), *p*=0.000026 using Poisson analysis; n= 5 mice per dilution and treatment, analysis was performed using ELDA (Extreme Limiting Dilution Assay) software [44]. (O) Colony formation of primary human AE/t(8;21) AML cells (*n*=6 individual patients). Colony number per sample following pharmacologic inhibition with CsA (5, 10 µM) compared to diluent control (NaCl 0.9%). (P) Representative pictures of colonies from t(8;21) AML bone marrow cells after pharmacological inhibition with cyclosporin A compared to diluent control (NaCl). Scale bars, 200 µm. (Q) Colony count of BM cells derived from 3 independent healthy donors. Colony number per sample following pharmacologic inhibition with CsA (5 µM) compared to diluent control (NaCl 0.9%). (R) Number of

hCD45-positive hCD13-positive cells per $1x10^6$ bone marrow (BM) cells after treatment with CsA (n=4 mice) compared to diluent control (NaCl 0.9%; n=4 mice). (S) Pie charts depicting engraftment of t(8;21) AML cells (%) after treatment with CsA or diluent control.

Figure 1

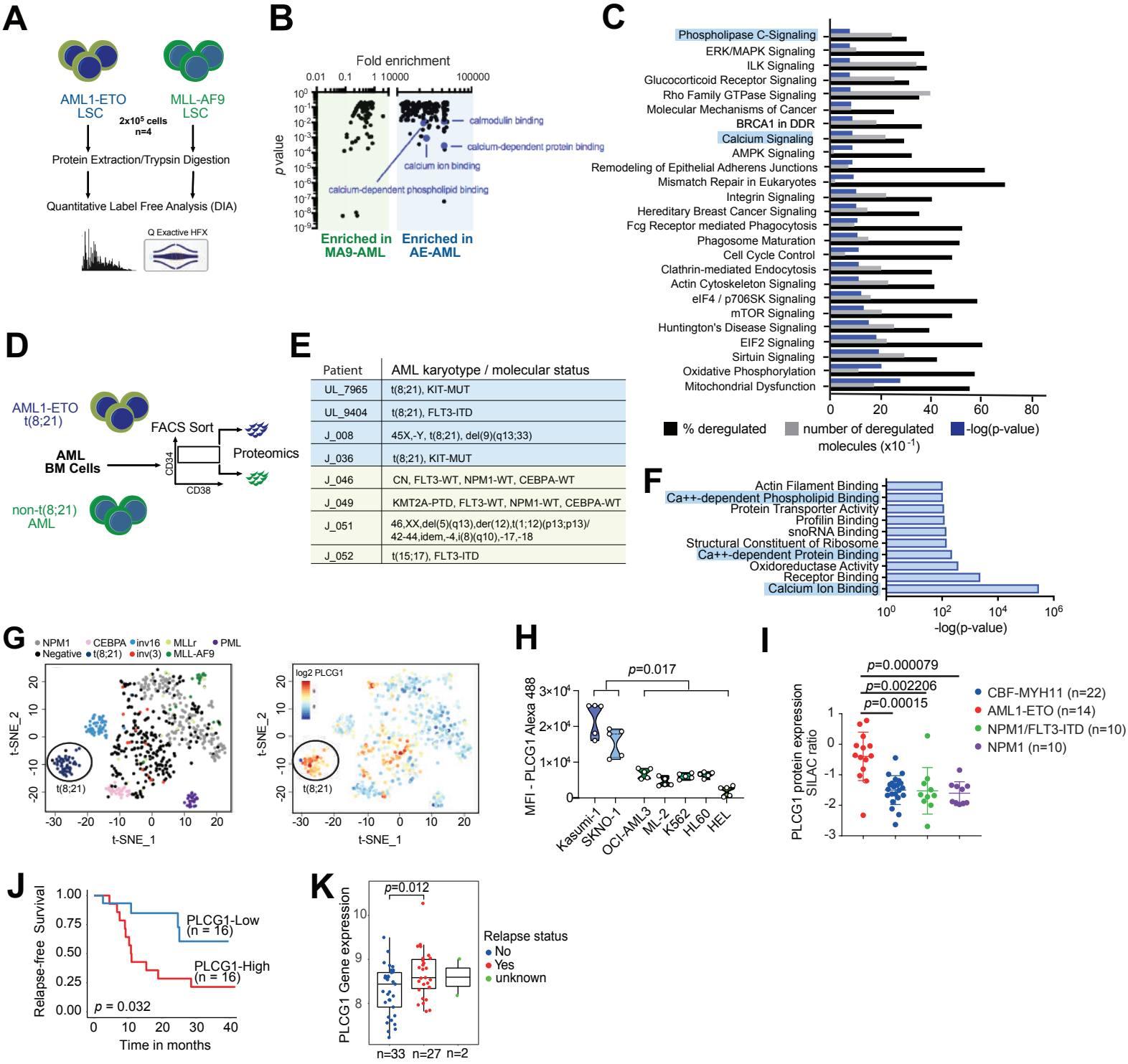

Patient	AML karyotype / molecular status
UL_7965	t(8;21), KIT-MUT
UL_9404	t(8;21), FLT3-ITD
J_008	45X,-Y, t(8;21), del(9)(q13;33)
J_036	t(8;21), KIT-MUT
J_046	CN, FLT3-WT, NPM1-WT, CEBPA-WT
J_049	KMT2A-PTD, FLT3-WT, NPM1-WT, CEBPA-WT
J_051	46,XX,del(5)(q13),der(12),t(1;12)(p13;p13)/ 42-44,idem,-4,i(8)(q10),-17,-18
J_052	t(15;17), FLT3-ITD

Figure 2

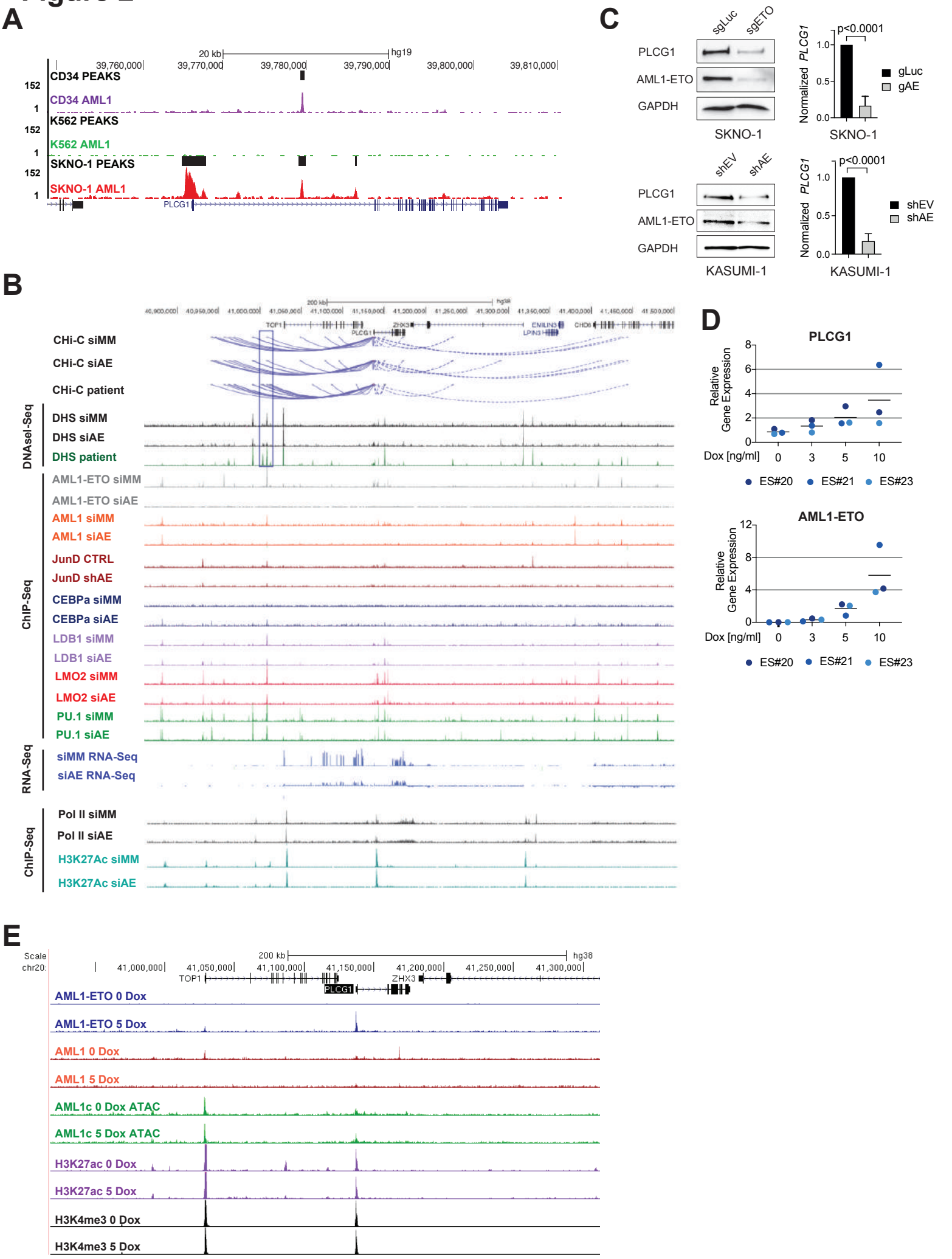
A
20 kb
hg19
39,760,000
39,770,000
39,780,000
39,790,000
39,800,000
39,810,000
CD34 PEAKS
CD34 AML1
K562 PEAKS
K562 AML1
SKNO-1 PEAKS
SKNO-1 AML1
PLCG1
B
CHi-C siMM
CHi-C siAE
CHi-C patient
DNAseI-Seq
DHS siMM
DHS siAE
DHS patient
ChIP-Seq
AML1-ETO siMM
AML1-ETO siAE
AML1 siMM
AML1 siAE
JunD CTRL
JunD shAE
CEBPa siMM
CEBPa siAE
LDB1 siMM
LDB1 siAE
LMO2 siMM
LMO2 siAE
PU.1 siMM
PU.1 siAE
RNA-Seq
siMM RNA-Seq
siAE RNA-Seq
ChIP-Seq
Pol II siMM
Pol II siAE
H3K27Ac siMM
H3K27Ac siAE
C
sgLuc
sgETO
PLCG1
AML1-ETO
GAPDH
SKNO-1
Normalized PLCG1
p<0.0001
gLuc
gAE
shEV
shAE
KASUMI-1
D
PLCG1
Relative Gene Expression
Dox [ng/ml]
ES#20
ES#21
ES#23
AML1-ETO
E
Scale
chr20:
200 kb
hg38
TOP1
ZHX3
AML1-ETO 0 Dox
AML1-ETO 5 Dox
AML1 0 Dox
AML1 5 Dox
AML1c 0 Dox ATAC
AML1c 5 Dox ATAC
H3K27ac 0 Dox
H3K27ac 5 Dox
H3K4me3 0 Dox
H3K4me3 5 Dox

Figure 3

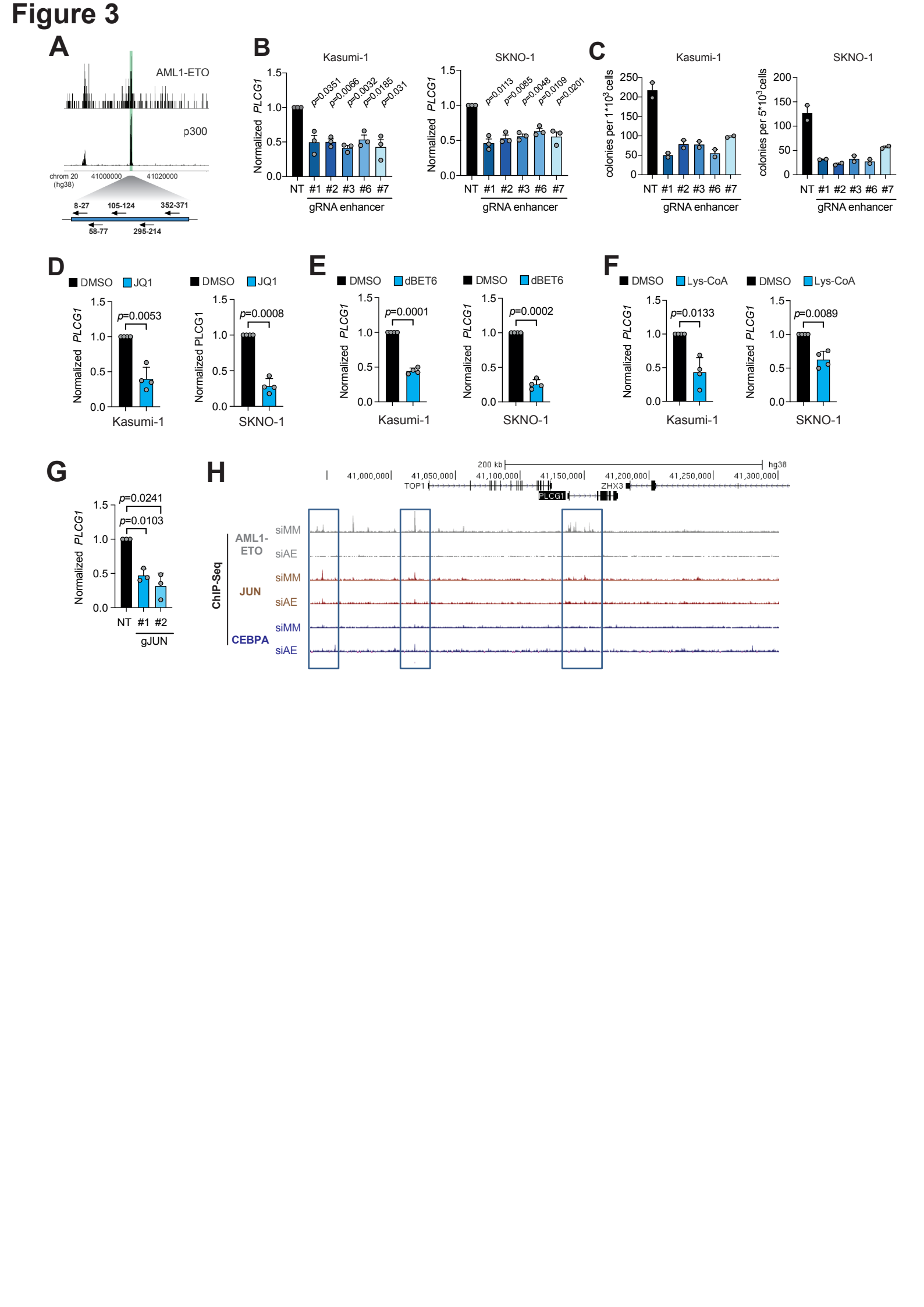
A
AML1-ETO
p300
chrom 20 (hg38)
41000000
41020000
8-27
105-124
352-371
58-77
295-214
B
Kasumi-1
SKNO-1
Normalized PLCG1
p=0.0351
p=0.0066
p=0.0032
p=0.0185
p=0.031
p=0.0113
p=0.0085
p=0.0048
p=0.0109
p=0.0201
NT #1 #2 #3 #6 #7
gRNA enhancer
C
Kasumi-1
SKNO-1
colonies per 1*10^3 cells
colonies per 5*10^3 cells
NT #1 #2 #3 #6 #7
gRNA enhancer
D
DMSO
JQ1
Normalized PLCG1
p=0.0053
p=0.0008
Kasumi-1
SKNO-1
E
DMSO
dBET6
Normalized PLCG1
p=0.0001
p=0.0002
Kasumi-1
SKNO-1
F
DMSO
Lys-CoA
Normalized PLCG1
p=0.0133
p=0.0089
Kasumi-1
SKNO-1
G
Normalized PLCG1
p=0.0241
p=0.0103
NT #1 #2
gJUN
H
200 kb
hg38
41,000,000
41,050,000
41,100,000
41,150,000
41,200,000
41,250,000
41,300,000
TOP1
ZHX3
PLCG1
ChIP-Seq
AML1-ETO
JUN
CEBPA
siMM
siAE

Figure 4

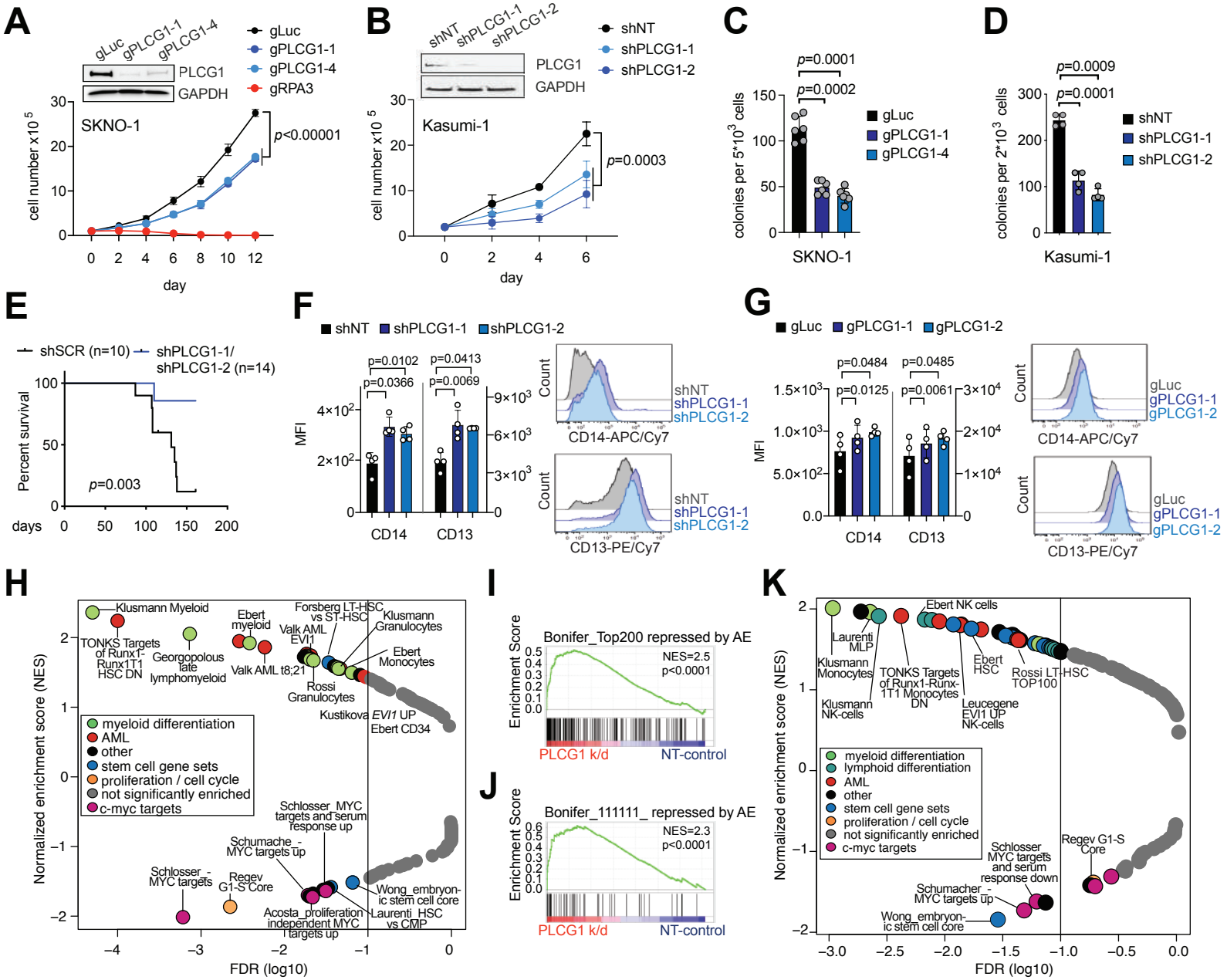
A
gLuc
gPLCG1-1
gPLCG1-4
gRPA3
PLCG1
GAPDH
SKNO-1
cell number x10 5
p<0.00001
day
B
shNT
shPLCG1-1
shPLCG1-2
Kasumi-1
p=0.0003
C
p=0.0001
p=0.0002
colonies per 5*10 3 cells
SKNO-1
D
p=0.0009
p=0.0001
colonies per 2*10 3 cells
Kasumi-1
E
shSCR (n=10)
shPLCG1-1/
shPLCG1-2 (n=14)
Percent survival
p=0.003
days
F
shNT
shPLCG1-1
shPLCG1-2
p=0.0102
p=0.0366
p=0.0413
p=0.0069
MFI
CD14
CD13
Count
CD14-APC/Cy7
CD13-PE/Cy7
G
gLuc
gPLCG1-1
gPLCG1-2
p=0.0484
p=0.0125
p=0.0485
p=0.0061
H
Klusmann Myeloid
TONKS Targets of Runx1-Runx1T1 HSC DN
Georgopolous late lymphomyeloid
Ebert myeloid
Valk AML t8;21
Valk AML EVI1
Forsberg LT-HSC vs ST-HSC
Klusmann Granulocytes
Ebert Monocytes
Rossi Granulocytes
Kustikova EVI1 UP
Ebert CD34
myeloid differentiation
AML
other
stem cell gene sets
proliferation / cell cycle
not significantly enriched
c-myc targets
Schlosser_MYC targets and serum response up
Schumache_-MYC targets up
Schlosser_-MYC targets
Regev G1-S Core
Wong_embryon-ic stem cell core
Acosta_proliferation independent MYC targets up
Laurenti_HSC vs CMP
Normalized enrichment score (NES)
FDR (log10)
I
Bonifer_Top200 repressed by AE
NES=2.5
p<0.0001
Enrichment Score
PLCG1 k/d
NT-control
J
Bonifer_111111_ repressed by AE
NES=2.3
p<0.0001
K
Ebert NK cells
Laurenti MLP
Klusmann Monocytes
Klusmann NK-cells
TONKS Targets of Runx1-Runx-1T1 Monocytes DN
Ebert HSC
Rossi LT-HSC TOP100
Leucegene EVI1 UP NK-cells
lymphoid differentiation
Schlosser MYC targets and serum response down
Schumacher_-MYC targets up
Wong_embryon-ic stem cell core
Regev G1-S Core

Figure 5

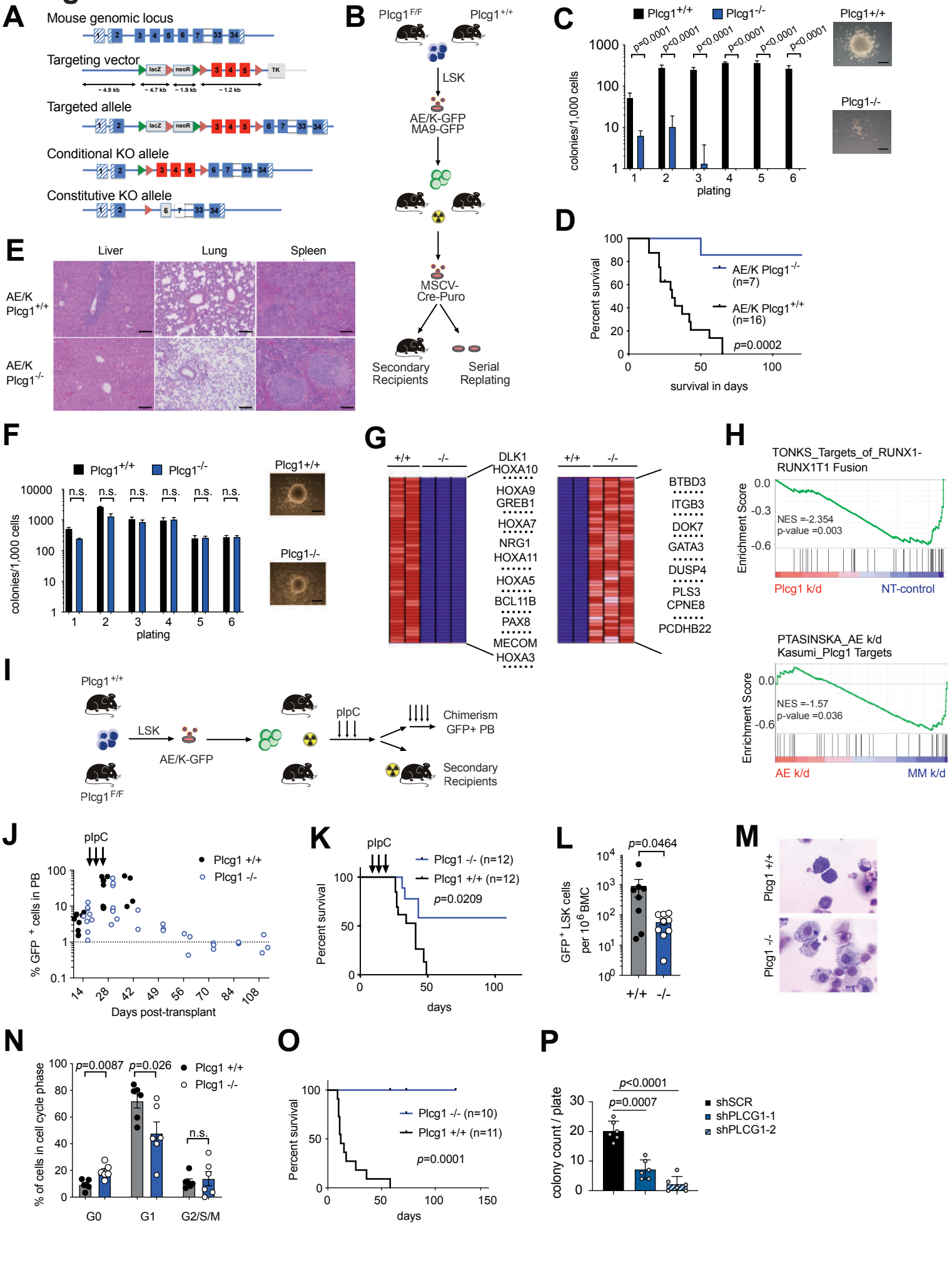
A
Mouse genomic locus
Targeting vector
lacZ
neoR
TK
~ 4.9 kb
~ 4.7 kb
~ 1.9 kb
~ 1.2 kb
Targeted allele
Conditional KO allele
Constitutive KO allele
B
Plcg1 F/F
Plcg1 +/+
LSK
AE/K-GFP
MA9-GFP
MSCV-
Cre-Puro
Secondary
Recipients
Serial
Replating
C
Plcg1+/+
Plcg1-/-
p=0.0001
p<0.0001
colonies/1,000 cells
plating
Plcg1+/+
Plcg1-/-
D
Percent survival
AE/K Plcg1 -/-
(n=7)
AE/K Plcg1 +/+
(n=16)
p=0.0002
survival in days
E
Liver
Lung
Spleen
AE/K
Plcg1 +/+
AE/K
Plcg1 -/-
F
Plcg1+/+
Plcg1-/-
n.s.
colonies/1,000 cells
plating
Plcg1+/+
Plcg1-/-
G
+/+
-/-
DLK1
HOXA10
HOXA9
GREB1
HOXA7
NRG1
HOXA11
HOXA5
BCL11B
PAX8
MECOM
HOXA3
BTBD3
ITGB3
DOK7
GATA3
DUSP4
PLS3
CPNE8
PCDHB22
H
TONKS_Targets_of_RUNX1-
RUNX1T1 Fusion
Enrichment Score
NES =-2.354
p-value =0.003
Plcg1 k/d
NT-control
PTASINSKA_AE k/d
Kasumi_Plcg1 Targets
Enrichment Score
NES =-1.57
p-value =0.036
AE k/d
MM k/d
I
Plcg1 +/+
LSK
AE/K-GFP
Plcg1 F/F
pIpC
Chimerism
GFP+ PB
Secondary
Recipients
J
pIpC
Plcg1 +/+
Plcg1 -/-
% GFP + cells in PB
Days post-transplant
K
pIpC
Plcg1 -/- (n=12)
Plcg1 +/+ (n=12)
p=0.0209
Percent survival
days
L
p=0.0464
GFP+ LSK cells
per 10 6 BMC
+/+
-/-
M
Plcg1 +/+
Plcg1 -/-
N
p=0.0087
p=0.026
Plcg1 +/+
Plcg1 -/-
n.s.
% of cells in cell cycle phase
G0
G1
G2/S/M
O
Plcg1 -/- (n=10)
Plcg1 +/+ (n=11)
p=0.0001
Percent survival
days
P
p<0.0001
p=0.0007
shSCR
shPLCG1-1
shPLCG1-2
colony count / plate

Figure 6

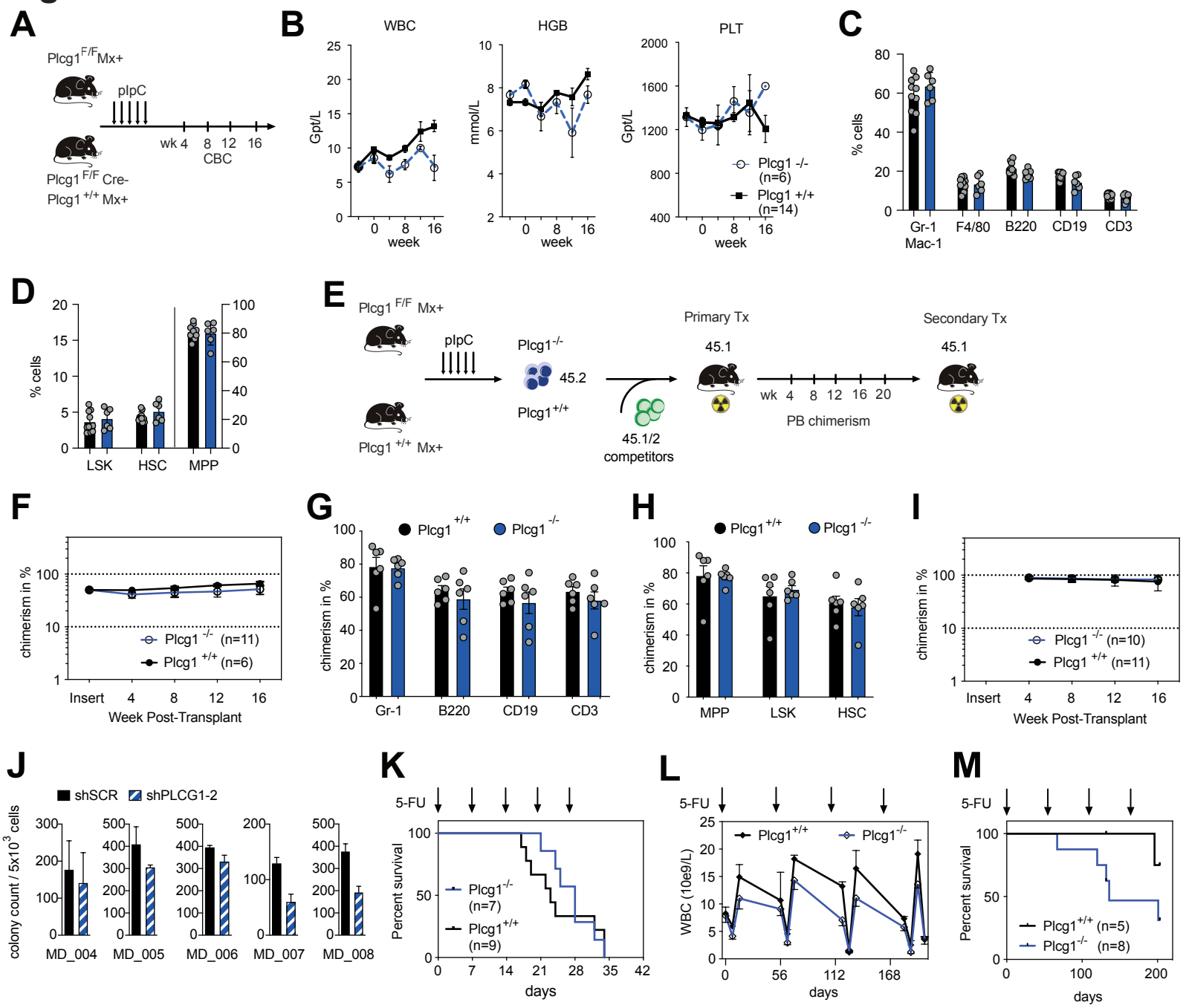
A
Plcg1F/FMx+
pIpC
wk 4 8 12 16
CBC
Plcg1F/F Cre-
Plcg1+/+ Mx+
B
WBC
HGB
PLT
Gpt/L
mmol/L
week
Plcg1 -/- (n=6)
Plcg1 +/+ (n=14)
C
% cells
Gr-1
Mac-1
F4/80
B220
CD19
CD3
D
% cells
LSK
HSC
MPP
E
Plcg1 F/F Mx+
pIpC
Plcg1-/-
45.2
Plcg1+/+
Plcg1 +/+ Mx+
45.1/2 competitors
Primary Tx
45.1
wk 4 8 12 16 20
PB chimerism
Secondary Tx
45.1
F
chimerism in %
Plcg1 -/- (n=11)
Plcg1 +/+ (n=6)
Insert 4 8 12 16
Week Post-Transplant
G
Plcg1 +/+
Plcg1 -/-
chimerism in %
Gr-1
B220
CD19
CD3
H
Plcg1 +/+
Plcg1 -/-
chimerism in %
MPP
LSK
HSC
I
chimerism in %
Plcg1 -/- (n=10)
Plcg1 +/+ (n=11)
Insert 4 8 12 16
Week Post-Transplant
J
shSCR
shPLCG1-2
colony count / 5x10^3 cells
MD_004
MD_005
MD_006
MD_007
MD_008
K
5-FU
Percent survival
Plcg1-/- (n=7)
Plcg1+/+ (n=9)
days
L
5-FU
Plcg1+/+
Plcg1-/-
WBC (10e9/L)
days
M
5-FU
Percent survival
Plcg1+/+ (n=5)
Plcg1-/- (n=8)
days

Figure 7

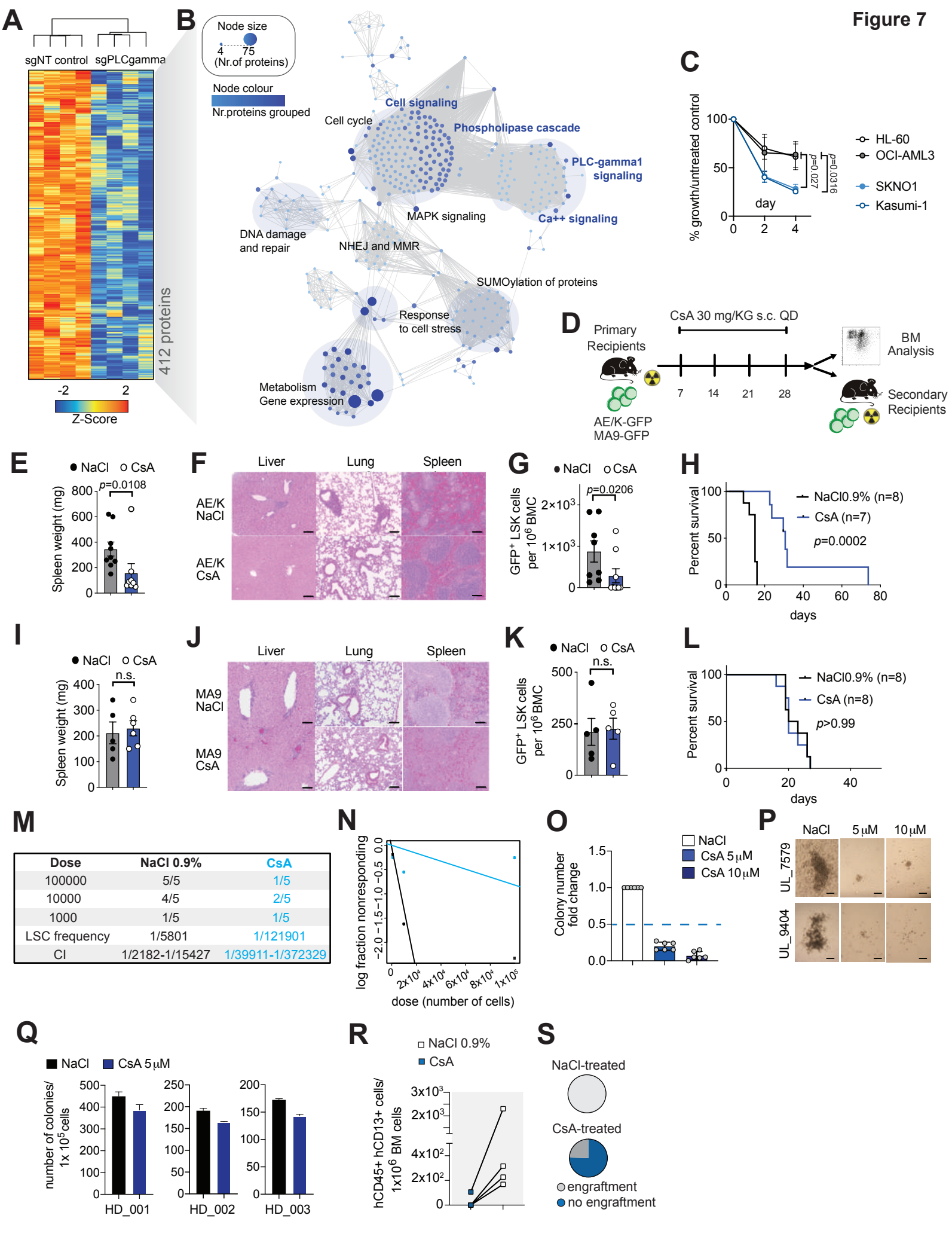

Dose	NaCl 0.9%	CsA
100000	5/5	1/5
10000	4/5	2/5
1000	1/5	1/5
LSC frequency	1/5801	1/121901
CI	1/2182-1/15427	1/39911-1/372329